Solvent Polarity Driven Helicity Inversion and Circularly Polarized Luminescence in Chiral Aggregation Induced Emission Fluorophores

Qiang Ye,‡[a,b] Feng Zheng,‡[c,d] Enqi Zhang,[a] Hari Krishna Bisoyi,[b] Shuyuan Zheng,[a] Dandan Zhu,[d] Qinghua Lu,*[d] Hailiang Zhang,[a] and Quan Li*[b]

[a]Key Laboratory of Polymeric Materials and Application Technology of Hunan Province, Key Laboratory of Environmentally-Friendly Chemistry and Applications of Ministry of Education, School of Chemistry, Xiangtan University, Xiangtan 411105, China

[b]Advanced Materials and Liquid Crystal Institute and Chemical Physics Interdisciplinary Program, Kent State University, Kent, OH 44242, USA

[c]School of Chemical Science and Engineering, Tongji University, Shanghai 200092, China

[d]School of Chemistry and Chemical Engineering, State Key Laboratory of Metal Matrix Composite, Shanghai Jiao Tong University, Shanghai 200240, China

‡These authors contributed equally to this work.

Table of Contents

Experimental Procedures

1.1 Materials

The chemical reagents were purchased from J&K Scientific Co. or Aldrich and used as received. Solvents were purchased from National Pharmaceutical Group Chemical Reagent Co. Tetrahydrofuran (THF), dichloromethane (DCM) and *n*-hexane (HEX) was dried over sodium and then distilled before use. Other solvents were used as received.

1.2 Measurements

The nuclear magnetic resonance (NMR) spectra were obtained from a MERCURY plus 400 (Varian, Inc., USA) using tetramethylsilane (TMS; δ=0) as internal reference. The high-resolution mass-spectrometric analysis was carried out by a Fourier Transform Ion Cyclotron Resonance Mass Spectrometer SolariX-70FT-MS (Bruker Daltonics, Germany). A Lambda 20 UV/Vis spectrometer (Perkin Elmer, Inc., USA) were employed to record UV/Vis spectra. The fluorescence spectra were measured using a LS 50B spectrometer (Perkin Elmer, Inc., USA). Quantum yields were measured on a QM/TM steady-state and time-resolved fluorescence spectrofluorometer (PTI Company, USA). The fluorescent images were taken when the assemblies were exposed under a commercially available UV lamp at 365 nm. The circular dichroism (CD) spectra were recorded using a JASCO J-815 circular dichroism spectrometer (JASCO, Japan). Circularly polarized luminescence was measured on a JASCO CPL-200 spectrometer (JASCO, Japan). All the CD and CPL data were accumulated by rotating the sample at different angles (0^o, 45^o, 90^o, 135^o, 180^o, 225^o, 270^o, 315^o). Scanning electron microscope (SEM) images were obtained on scanning electron microscope S-4800 (Hitachi, Japan). Transmission electron microscope (TEM) observation was carried out on JEM-2100 (JEOL Ltd., Japan).

1.3 Sample preparation

Assemblies film for CD and CPL test: Enantiotopic ***R*-** or ***S*-TPE-Ph-PEA** molecules were dissolved in pure DCM, and in different mixed solvent systems at a concentration of 10^{-4} M with DCM-HEX volume ratios of 1:9, 2:8, 3:7, 8:2, respectively. The solutions were cast onto quartz plate. After slow natural solvent evaporation, more solution was applied and the solvent evaporated, this process was repeated several times to generate the corresponding assembly films on substrate surfaces.

Assemblies for SEM imaging: Enantiotopic ***R*-** or ***S*-TPE-Ph-PEA** molecules were dissolved in pure DCM, and in different mixed solvent systems at a concentration of 10^{-4} M with DCM-HEX volume ratios of 1:9, 2:8, 3:7, 5:5, 8:2, respectively. The solutions were cast onto silicon slices and the solvent was removed via slow natural evaporation to generate the corresponding assemblies on the substrate surface.

Self-assembly process determination (TEM samples preparation): ***R*-** or ***S*-TPE-Ph-PEA** molecules were dissolved in DCM at a concentration of 10^{-4} M and followed by adding to 9 times volume of hexane (HEX) to prepare solution, respectively. The solutions were dropped onto the copper grid and after allowing different self-assembly time (2 min and 4 min after self-assembling), and the sample was moved into vacuum drying oven to evaporate solvent immediately.

1.4 Computational methods

1.4.1 Conformational analysis

Conformation analysis was performed using "Conformers" module[1] as implemented in BIOVIA Materials Studio 2019. All of the calculations were carried out using system grid scanning method with the condensed-phase optimized molecular potentials for atomistic simulation studies (COMPASSII) force field[2]. Coulomb and van der Waals (vdW) interactions were calculated by Ewald method. ϕ1 and ϕ2 (see Figure S13-14) were varied by 10 degrees per step, *i.e.*, the total calculation steps were 36. The calculation accuracy was set to "ultra-fine", and other parameters were set to the default value of the program.

1.4.2 Density functional theory (DFT) calculations

DFT calculations were carried out using the Conductor-like Screening Model (COSMO) solvation model[3]. The nonlocal generalized gradient approximation (GGA) exchange-correlation functional was employed in all geometry optimizations, viz., the PW91 functional of Perdew and Wang[4]. DMol^3 utilizes a basis set of numeric atomic functions, which are exact solutions to the Kohn-Sham equations for the atoms [5]. Gaussian functions have been demonstrated to have small basis set superposition errors. In the present study an all-electron polarized split valence basis set, termed double numeric polarized with the large basis set (DNP 3.5) was used. The tolerance for convergence of the self-consistent field (SCF) density was set to 1 x 10^{-5} hartrees, while the tolerance for energy convergence was set to 1 x 10^{-6} hartrees. Additional convergence criteria include the tolerance for converged gradient (0.002 hartrees/ Å) and the tolerance for converged atom displacement (0.005 Å). To enhance SCF convergence efficiency during optimization of stationary points, a small electron thermal smearing value of 0.005 Ha was specified for all calculations unless explicitly stated to the contrary. The thermal smearing option in Materials Studio makes use of a fractional electron occupancy scheme at the Fermi level according to a finite-temperature Fermi function[6]. In all cases optimized geometries were subjected to full frequency analyses at the same GGA/PW91/DNP level of theory to verify the nature of the stationary points. Equilibrium geometries were characterized by the absence of imaginary frequencies. The reported energies (in kcal/mol) refer to Gibbs free energies at 298.15 K and 1 atm.

1.4.3 Prediction of possible packing models

In flexible molecules due to single bond rotation, conformational polymorphism is commonly observed, where a molecule can adopt different conformations through a controlled crystallization process[7]. Computational method of polymorph prediction has become an important area[7,8]. In current study, polymorph prediction of the most likely packingmodels was carried out using "Polymorph" module[9] in MS software. "Clustering" and "Packing" modes were selected simultaneously. The maximum cluster

number was set to 500. The calculations were performed under COMPASSII force field with all "Space Groups"[10] available in MS. Finally, the Reflex Module[11] in MS was used to simulate the X-ray diffraction (XRD) spectrum of the simulated packing models. By comparing with the experimental XRD pattern, the most likely packing models were found, which were used to get insight into the molecular packing information of the self-assembly systems.

Experimental Data

2.1 Optical properties

Figures 2a and S4a show the UV/vis absorption spectra of ***S*-** and ***R*-TPE-Ph-PEA**. Absorption bands at 277 nm and 341 nm corresponded to the π-π* transition of chiral PEA moieties and π-π* transition of TPE moieties, respectively. The maximums absorption extinction coefficients are 2.17×10^4 L*mol-1*cm^{-1} and 2.21×10^4 L*mol^{-1}*cm^{-1} to ***S*-** and ***R*-TPE-Ph-PEA**, respectively. The quantum yields of ***S*-** and ***R*-TPE-Ph-PEA** in solid state were measured by steady-state and time-resolved fluorescence spectrofluorometer with 16 nm integrating sphere and presented high values of 40% and 40.5%, respectively. To investigate molecular aggregation behaviors in solution, concentration dependent absorption spectra (Figure S1) were studied in DCM. When concentration is lower than 2.5×10^{-5} M, both ***S*-** and ***R*-TPE-Ph-PEA** follow Lambert-Beer's law, meaning molecular still be well dispersed in solution. But when concentration comes to 5×10^{-5} M, both ***S*-** and ***R*-TPE-Ph-PEA** show some deviation to Lambert-Beer's law, indicating molecules would already aggregate due to extended pi-conjugation of TPE moieties. To further verify the aggregation-induced luminescence properties, fluorescence emission spectra of ***S*-** and ***R*-TPE-Ph-PEA** in THF/water mixtures with different ratios were also studied (see PL spectra shown in Figures S2a, 2b). When the ratio of water (poor solvent) increased up to 80%, emission at 470 nm was observed in the spectra. When the ratio of water kept increasing, the PL intensities dramatically enhanced, implying ***S*-** and ***R*-TPE-Ph-PEA** exhibited typical AIE property. These results indicated the ***S*-** and ***R*-TPE-Ph-PEA** still preserves the AIE feature.

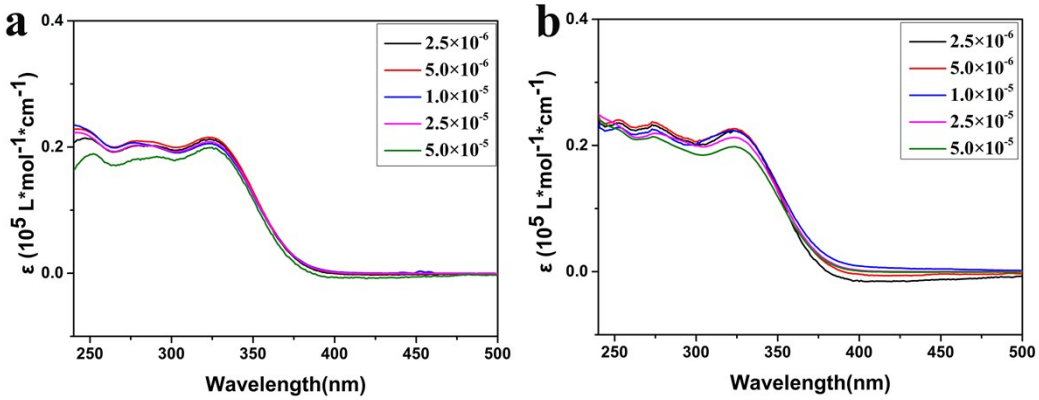

Figure S1. Concentration dependent absorption spectra of ***S*-** (a) and ***R*-TPE-Ph-PEA** (b) in DCM.

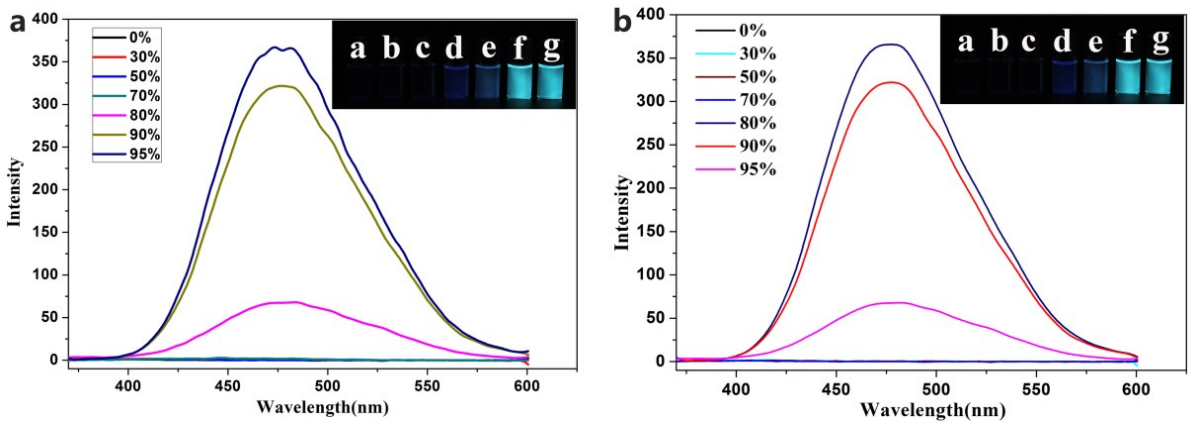

Figure S2. Aggregation-induced luminescence property of ***S*-** (a) and ***R*-TPE-Ph-PEA** (b), which was dissolved in mixed solution of THF/water at a concentration of 5×10^{-6} M (Water; 0%, 30%, 50%, 70%, 80%, 90%, 95%). Excitation wavelength: λex = 345 nm, λem = 470 nm.

2.2 Chiroptical properties

To confirm the cast films uniform and stable, AFM (atomic force microscope) is used to analysis cast films (Figure S3). Both ***S*-** and ***R*-TPE-Ph-PEA** cast films from different assembly condition show small surface roughness and few defects, we believe cast films are uniform and stable enough to study their optical properties.

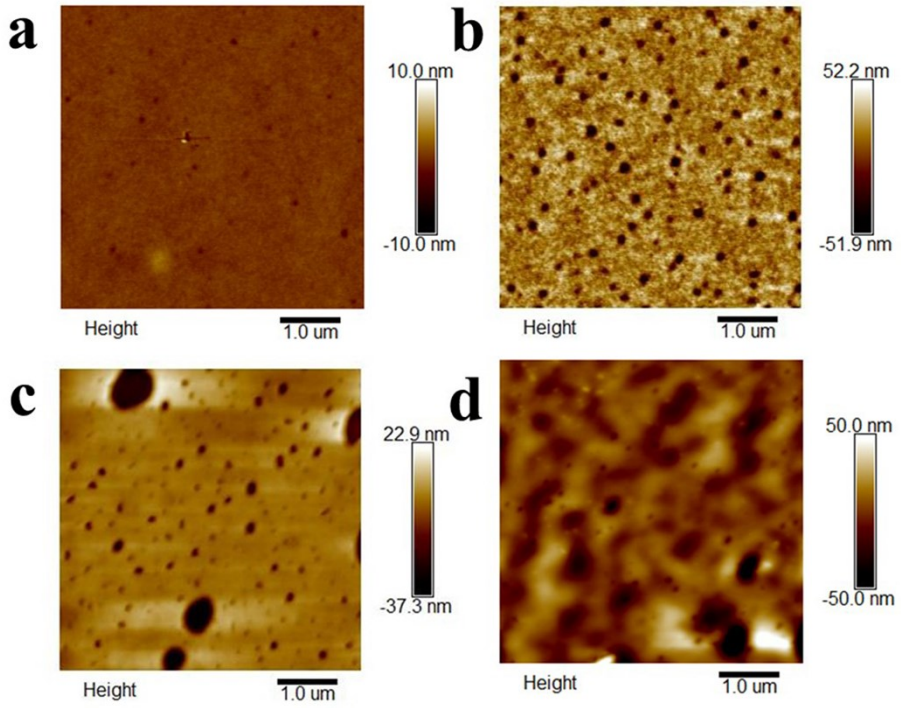

Figure S3. AFM(atomic force microscope) morphology pictures of ***S*-** and ***R*-TPE-Ph-PEA** assembly films obtained from different solution (1×10^{-4} M) (a) DCM, ***S*-TPE-Ph-PEA** , (b) DCM/HEX 1:9, ***S*-TPE-Ph-PEA**, (c) DCM, ***R*-TPE-Ph-PEA**, (d) DCM/HEX 1:9, ***R*-TPE-Ph-PEA**.

To eliminate test errors resulting from anisotropy in samples, all the CD and CPL data were accumulated by rotating the sample at different angles (0^o, 45^o, 90^o, 135^o, 180^o, 225^o, 270^o, 315^o).

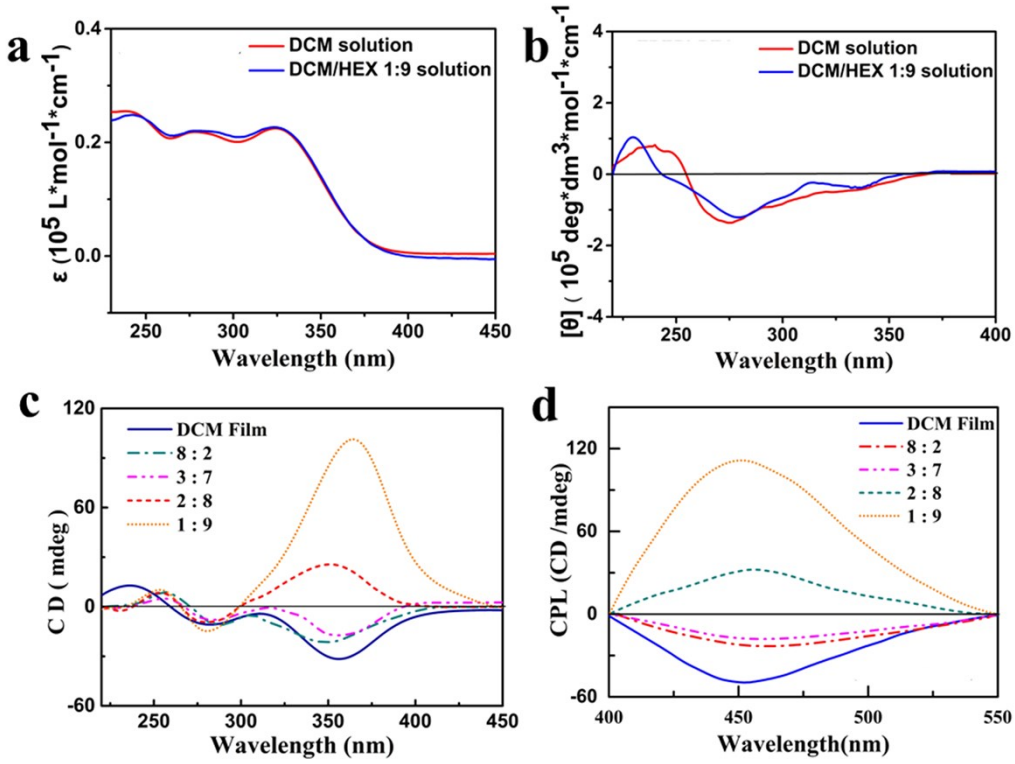

Figure S4. UV (a) spectra and circular dichroism (b) of ***R*-TPE-Ph-PEA** in solution(concentration: 5×10^{-6} M); Circular dichroism(c) and circularly polarized luminescence (d) of ***R*-TPE-Ph-PEA** assembly films obtained from different solution: DCM (blue); DCM/HEX(vol/vol) 8:2 (cyan); DCM/HEX 3:7 (pink), DCM/HEX 2:8 (red), DCM/HEX 1:9 (orange).

In general, the dissymmetry factor value for absorption (g_{abs}) could be expressed as follows: $g_{abs} = \Delta\varepsilon/\varepsilon = (\varepsilon_L - \varepsilon_R)/\varepsilon = 2(\varepsilon_L - \varepsilon_R)/(\varepsilon_L + \varepsilon_R)$, where ε_L and ε_R are the left- and right-handed molar extinction coefficients, respectively. The UV spectra (Figures S5a, b) and g_{abs} curves (Figures S5c, d) of ***S*-** and ***R*-TPE-Ph-PEA** assemblies were consistent with their CD spectra (Figures 4c, S4c). The dissymmetry factor curves reveal that both ***S*-** and ***R*-TPE-Ph-PEA** had high g_{abs} values in DCM/HEX 1:9 assembling film, with high average g_{abs} values of -0.078 and -0.074 at 370 nm, respectively, corresponding to the absorption band of TPE moieties.

Circular dichroism spectra in solution showed that the chirality of ***R*-TPE-Ph-PEA** in DCM/HEX (1:9) were not changed by comparing with DCM solution（Figure S4b）. These results indicated that the molecular chiral configuration of ***S*-** and ***R*-TPE-Ph-PEA** were both stable in solution rather than handedness inversed in DCM/HEX (1:9) or (2:8) assemblies. Therefore, it provided a direct evidence that handedness inversion in different ***S*-** and ***R*-TPE-Ph-PEA** assemblies were not originated from the breaking of molecular chiral balance.

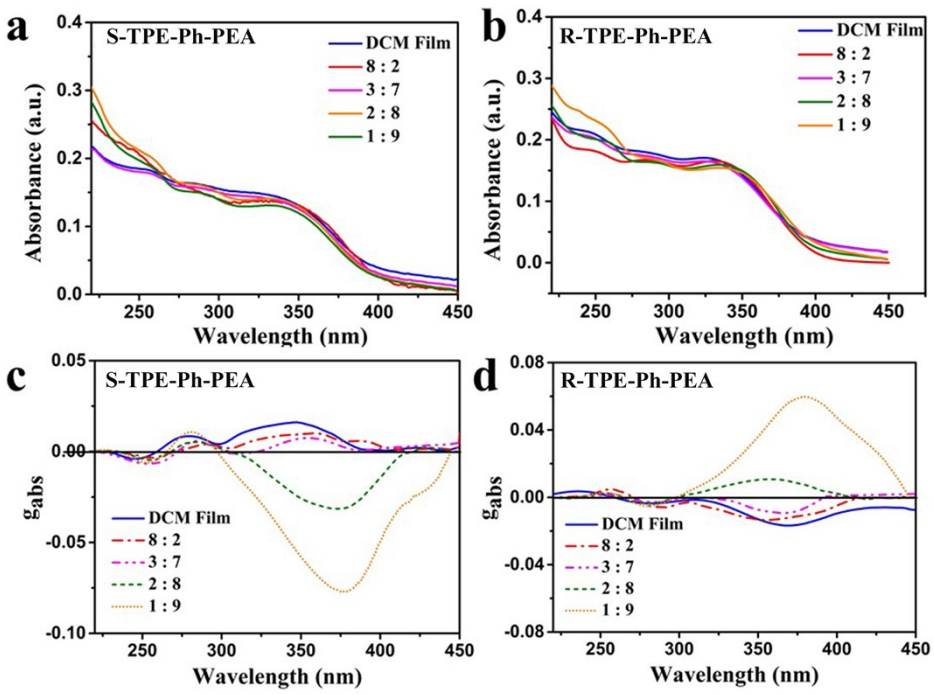

Figure S5. UV spectra (a, b) and g_{abs} curves (c, d) of ***S*-TPE-Ph-PEA** and ***R*-TPE-Ph-PEA** assemblies obtained from different solution in DCM (blue); DCM/HEX(vol/vol) 8:2 (cyan); DCM/HEX 3:7 (pink), DCM/HEX 2:8 (red), DCM/HEX 1:9 (orange) after solution (10^{-4} M) evaporation.

The performance of CPL-active materials can be quantitatively evaluated using g_{lum}, which is defined as $2(I_L - I_R)/(I_L + I_R)$, where I_L and I_R are the luminescence intensities of left- and right-handed polarized light, respectively. The fluorescence (FL) spectra (Figures S6a, b) and glum curves (Figures S6c, d) of ***S*-** and ***R*-TPE-Ph-PEA** assemblies are in accord with CPL spectra (Figures 2d, S4d), respectively. The g_{lum} curves showed that ***S*-** and ***R*-TPE-Ph-PEA** had the maximum value of -0.27 and 0.26 in DCM/HEX = 1:9 assembling film, respectively. The CD and CPL dissymmetry factor values of ***S*-** and ***R*-TPE-Ph-PEA** assemblies had similar behavior when varying the ratio of DCM/HEX. The assemblies with high order structure gain high value.

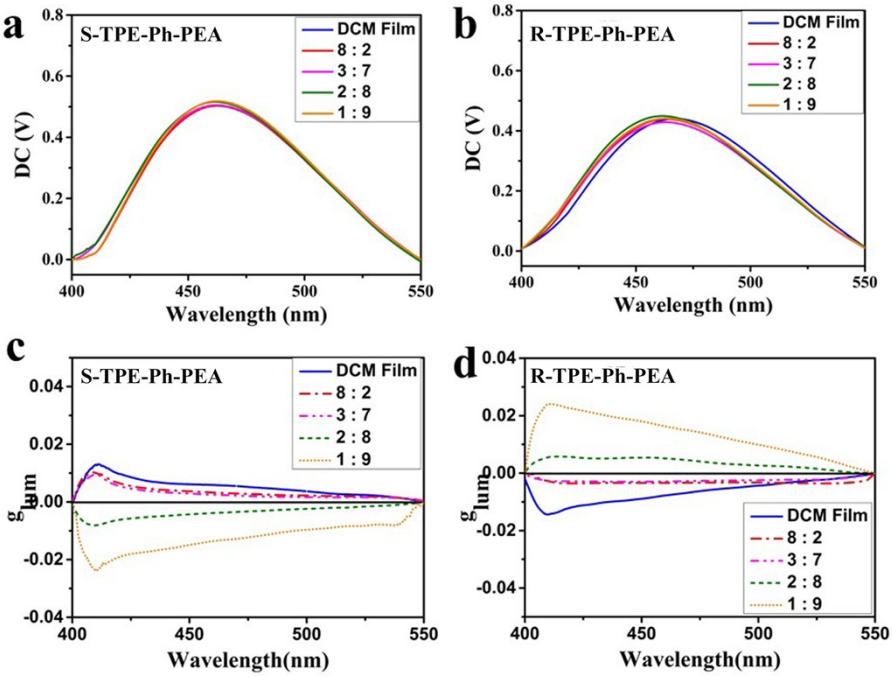

Figure S6. Fluorescence spectra (a, b) and g_{lum} curves (c, d) of ***S***- and ***R*-TPE-Ph-PEA** assemblies obtained from different solution in DCM (blue); DCM/HEX(vol/vol) 8:2 (cyan); DCM/HEX 3:7 (pink), DCM/HEX 2:8 (red), DCM/HEX 1:9 (orange) at a concentration of 0.5mg/ml (λex =345 nm).

2.3 SEM pictures of *R*-TPE-Ph-PEA assemblies

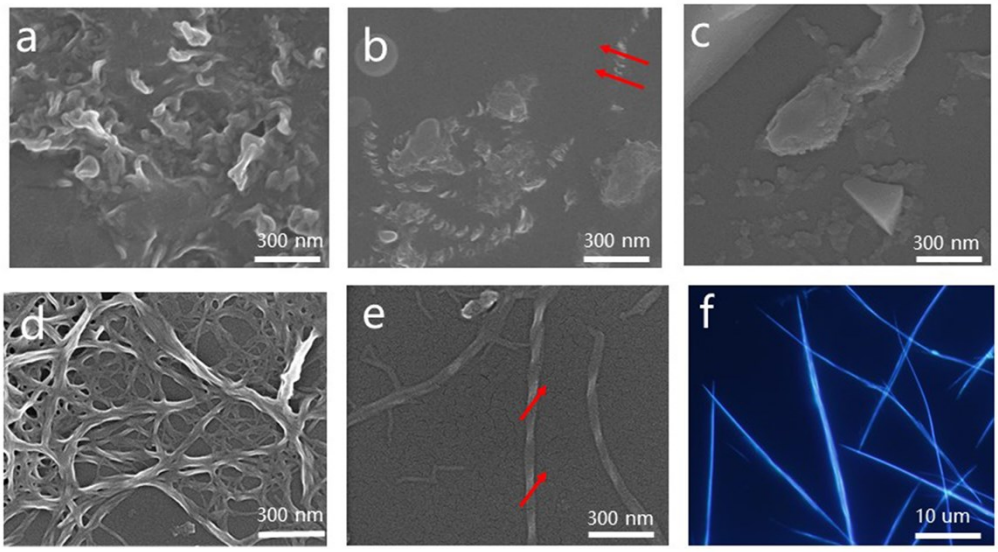

Figure S7. SEM images of ***R*-TPE-Ph-PEA** assemblies obtained from DCM/HEX mixtures with different ratios a) DCM; b) 8 : 2; c) 3 : 7; d) 2 : 8; e) 1 : 9. f)Confocal fluorescence microscope image of ***R*-TPE-Ph-PEA** assemblies obtained from DCM/HEX solution with ratio of 1:9

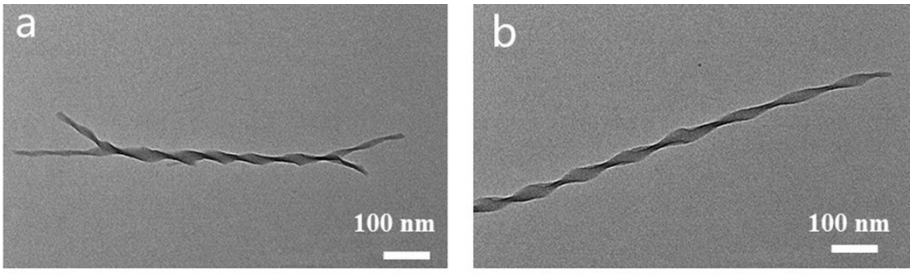

Figure S8. TEM images of ***R*-TPE-Ph-PEA** assemblies from DCM/HEX 1:9 system after self-assembling for 2 min (a) and 4 min (b) illustrating the formation and growth of helical fibers of ***R*-TPE-Ph-PEA** assemblies from solutions with concentration of 1×10^{-4} M.

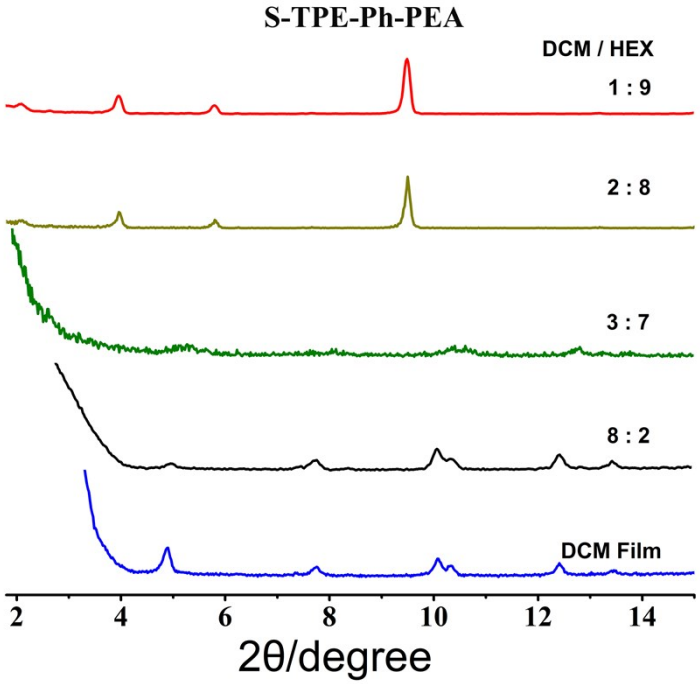

Figure S9. XRD patterns of ***S*-TPE-Ph-PEA** assemblies as cast films obtained from DCM/HEX (0.5mg/ml) on silicon wafer substrates.

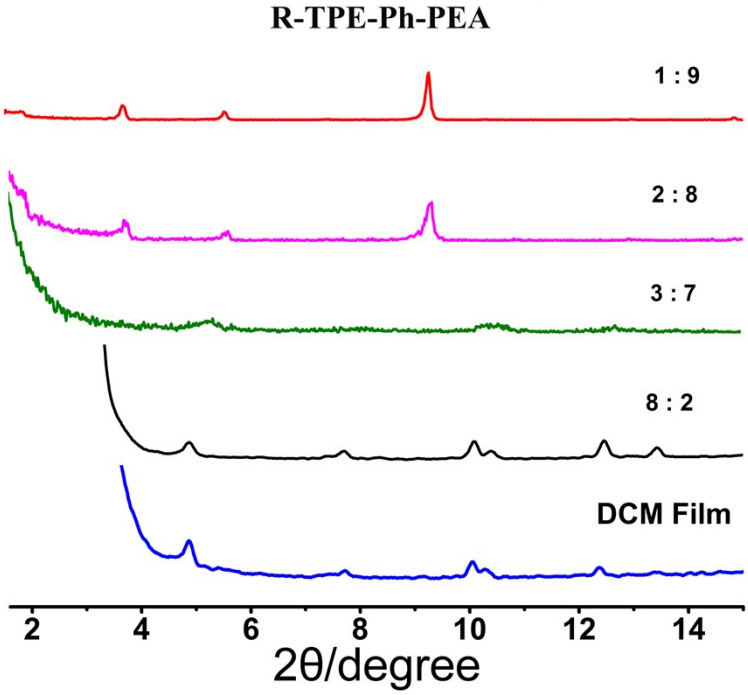

Figure S10. XRD patterns of ***R*-TPE-Ph-PEA** assemblies as cast films obtained from DCM/HEX (0.5mg/ml) on silicon wafer substrates.

X-ray diffraction (XRD) technique and structural simulation were harnessed to understand the molecular packing in the supramolecular helical assemblies. Single crystals of ***S*-** and ***R*-TPE-Ph-PEA** compounds did not be obtained though generous methods were tried. This could be because ***S*-** and ***R*-TPE-Ph-PEA** compounds are insoluble in hexane, while two different conformers could co-exist in DCM (according to our computational results). The XRD diffractogram of ***S*-** and ***R*-TPE-Ph-PEA** as cast films in Figures S9 and S10 shows the characteristic *d*-spacings in different assembly condition of 4.45 nm, 2.25 nm, 1.57 nm, 0.92 nm by DCM/HEX 1:9, the strong and sharp diffraction peaks indicated a high degree of order (crystalline) in assembly. With reduction of the ratio of DCM/HEX to 2/8, the position of diffraction peaks almost unchanged but the intensity decreased rapidly, which implied the assembly order declined. However, the crystallization of the **TPE-Ph-PEA** assembly was sufficiently disrupted when the ratio of DCM/HEX reached to 3:7, leading to either an amorphous network or aggregated sheets/films with non-ordered interlayer orientation. This was indicated by the two weak and broad diffraction peaks corresponding to 1.67 and 0.83 nm in the XRD pattern. The film dried from DCM/HEX 8:2 and DCM showed diffraction patterns with similar peak positions at *d*-spacing of 1.76 nm, 1.16 nm, 0.87 nm, 0.84 nm, 0.71 nm, 0.66 nm, meaning both ***S*-** and ***R*-TPE-Ph-PEA** assemble from DCM/HEX 8:2 and DCM with order structures.

2.3 Computational results

According to the IUPAC-IUB[12] recommendation, dihedral or torsional angles were specified with -180 and 180^{o} for both backbone (ϕ1, ϕ2) conformations (Figure S11). Conformation analysis for ***R*-** and ***S*-TPE-Ph-PEA** molecules were performed using "Conformers" module[1] as implemented in BIOVIA Materials Studio 2019. Rotational barriers are depicted in Figures S12 and S13. The conformers with lowest energy as shown in Figures S14 and S15 were then subject to geometry optimization using the $DMol_3$ DFT code[13]. To account for the interaction of polar (DCM) and nonpolar (Hexane) solvents on ***R*-** and ***S*-TPE-Ph-PEA**, calculations were carried out using the COSMO solvation model[3].

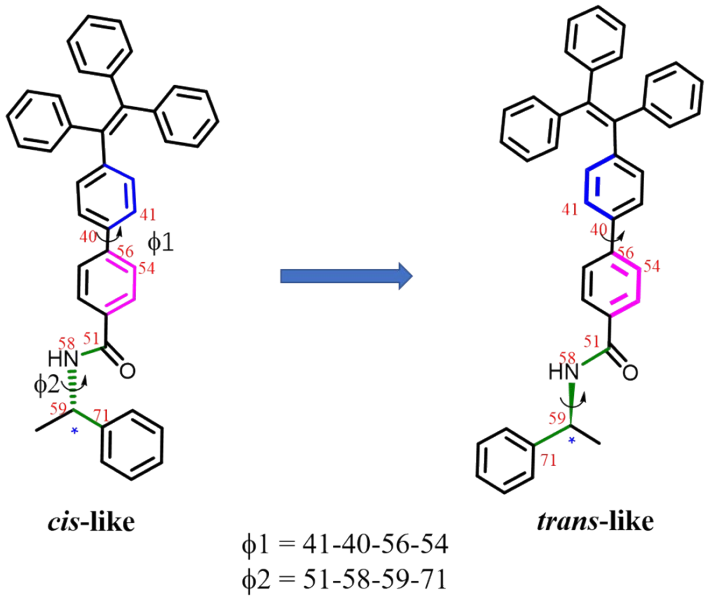

Figure S11. Numbering of the atoms and dihedral angles for ***S*-TPE-Ph-PEA.** The dihedral angles are defined in terms of the atoms involved.

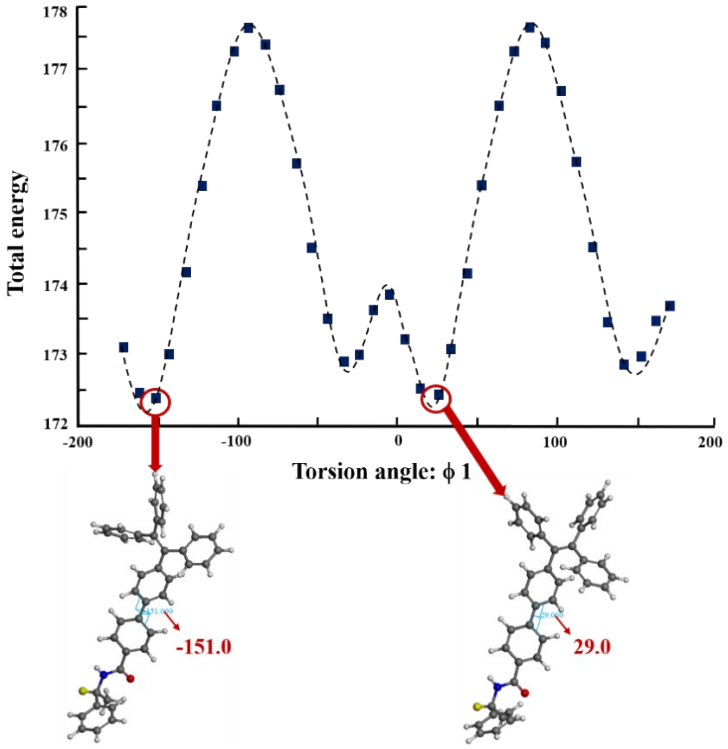

Figure S12. Potential energy scan (PES) on the ***S*-TPE-Ph-PEA** molecule by varying the degree of ϕ1.

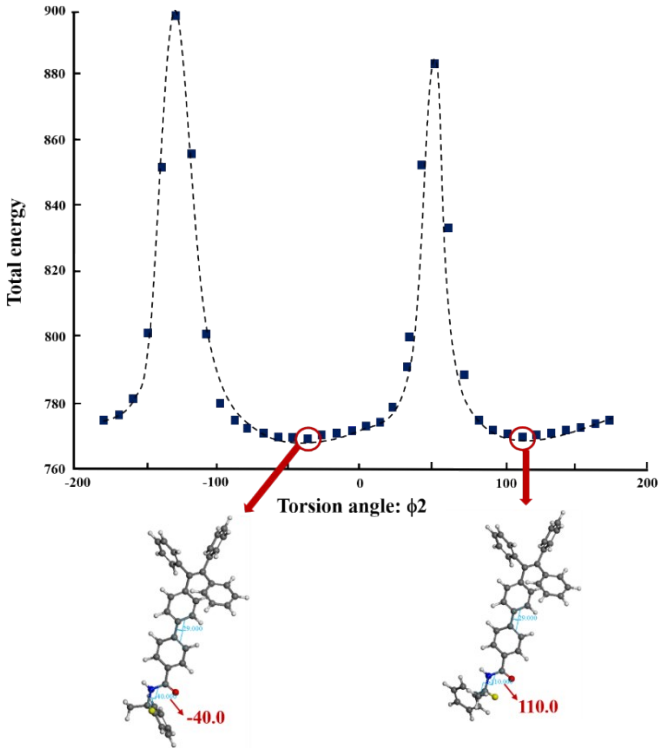

Figure S13. Potential energy scan (PES) on the ***S*-TPE-Ph-PEA** molecule by varying the degree of ϕ2.

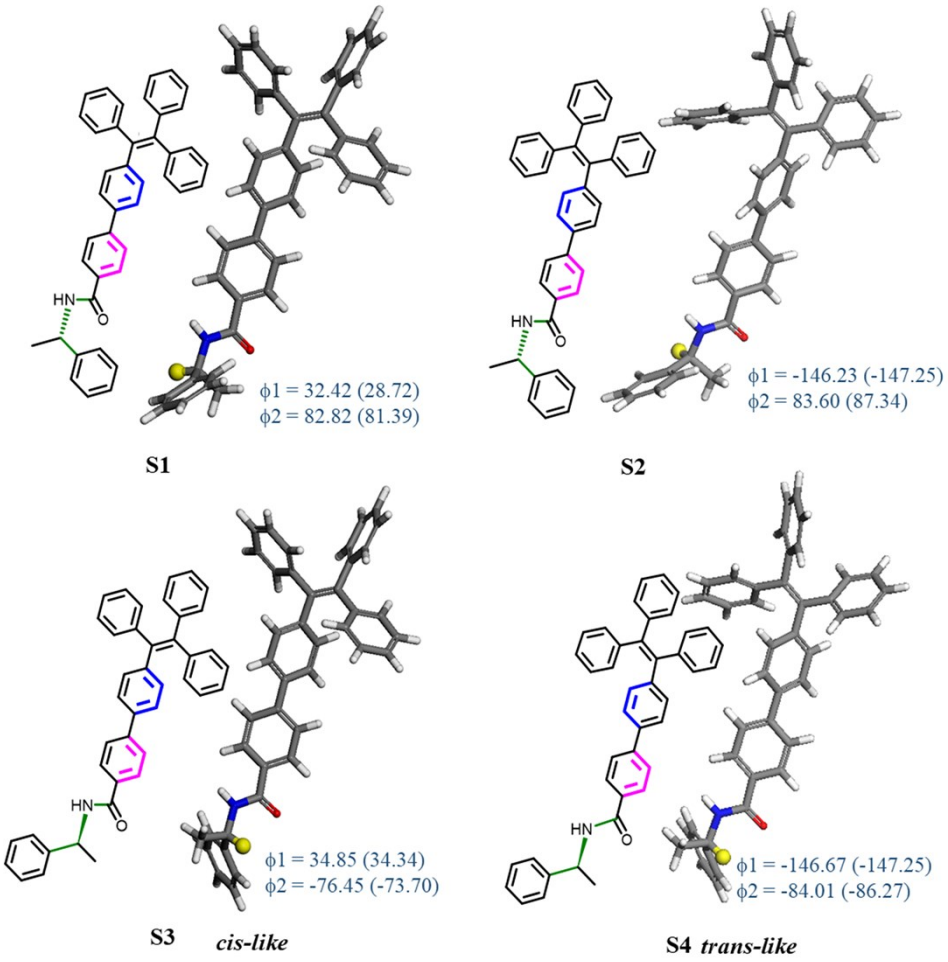

(a)

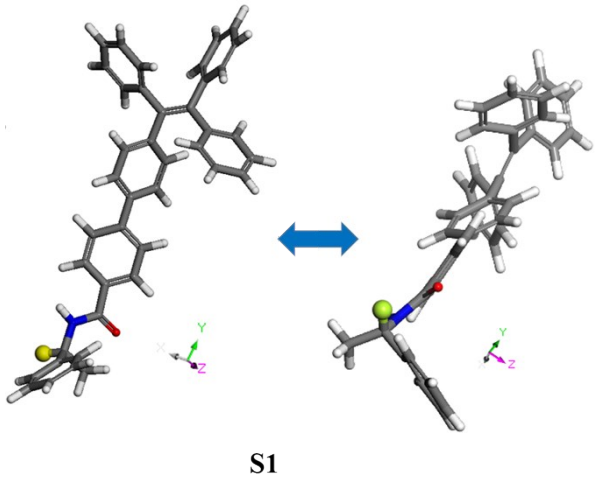

(b)

Figure S14. (a) DFT optimized structures of four most stable conformers for ***S*-TPE-Ph-PEA in DCM (hexane) solvation model** , and the degree of dihedral angles. The notation of each conformation based on the degree of ϕ1 and ϕ2. **S1** represents the conformer with 0<ϕ1<90 and ϕ2<0, **S2** for -180<ϕ1<-90 and ϕ2<0, **S3** for 0<ϕ1<90 and ϕ2>0, while **S4** for -180<ϕ1<-90 and ϕ2>0. (b) Molecule in left-handed configuration.

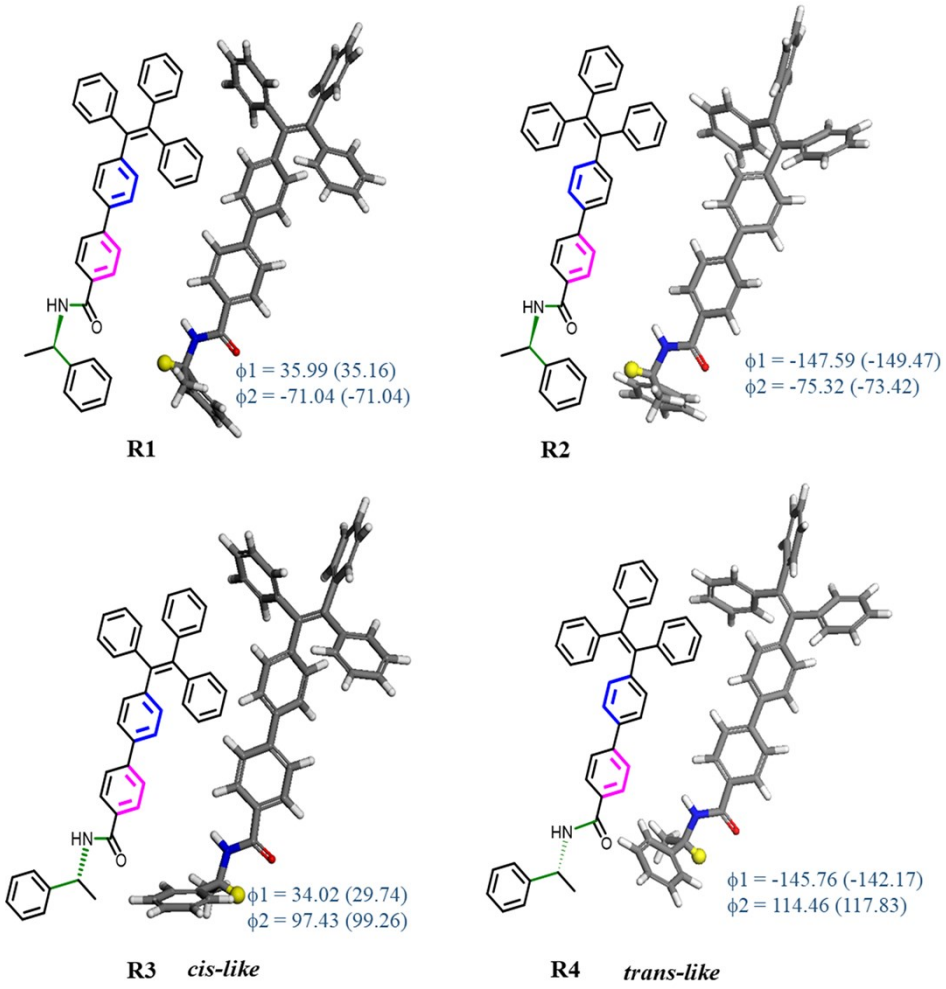

(a)

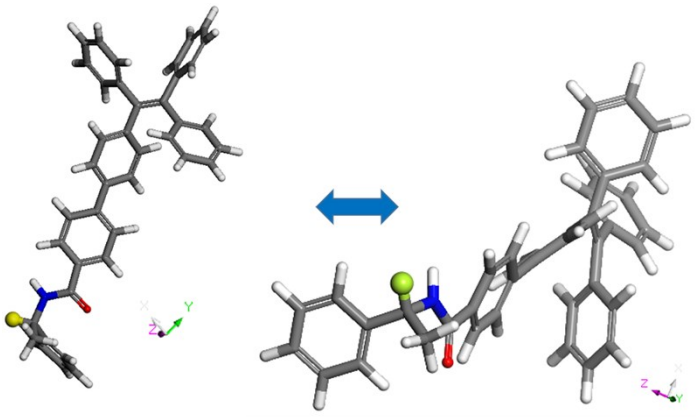

(b)

Figure S15. (a) DFT optimized structures of four most stable conformers for ***R*-TPE-Ph-PEA in DCM (hexane) solvation model**, and the degree of dihedral angles. The notation of each conformation based on the degree of ϕ1 and ϕ2. The same notation manner as ***S*-TPE-Ph-PEA** was applied to ***R*-TPE-Ph-PEA**. (b) Molecule in right-handed configuration.

Table S1. Molecular length (Å) and relative Gibbs free energy (kcal/mol) for all stable conformations.

	conformer	Solvation model			
		DCM		Hexane	
		Molecular length（Å）	ΔG1（kcal/mol）	Molecular length（Å）	ΔG1（kcal/mol）
***S*-TPE-Ph-PEA**	**S1**	21.2	-2.0	21.3	-0.1
	S2	21.3	-1.3	20.8	-0.4
	S3	21.7	-3.9	21.7	-1.9
	S4	21.3	-3.3	21.8	-3.5
***R*-TPE-Ph-PEA**	**R1**	19.8	0.0	19.9	0.0
	R2	21.0	-0.4	21.0	0.6
	R3	21.3	-6.8	21.3	-3.5
	R4	20.8	-5.8	20.7	-4.6

1 ΔG: Gibbs free energy relative to **R1**

Simulated packing models

We envisioned that we could predict the possible packing models of ***R*-** and ***S*-TPE-PEA** molecules according to the experimental powder XRD patters, and thereby to get insight into the molecular packing information of the helical assemblies. Computational models for the most stable conformers in hexane, **S4** and **R4** were minimized using COMPASSII force field in different space groups using Materials Studio 2019 software[9,10], and the corresponding simulated XRD patters were generated (Figure S16). It is shown in Figure S17 that the simulated packing models for S4 has head-to-tail arrangement in a unit cell (b), and the molecules are packed to form a chain-like structure with left helix (c). Similar simulated packing was obtained for **R4** as shown in Figure S18a. The H-bonding interactions make the molecules to form a chain-like structure with right helix as shown in Figure S18b. Similar simulations were performed to predict the possible packing models for both compounds in DCM based on their experimental powder XRD patterns. The simulated XRD pattern is shown in Figure S19. It corresponds to the predicted packing model as shown in Figure S20, where the most stable conformer **S3** in DCM assembles in film form. As R compound has similar XRD pattern, the possible packing model could be similar as that of **S3**.

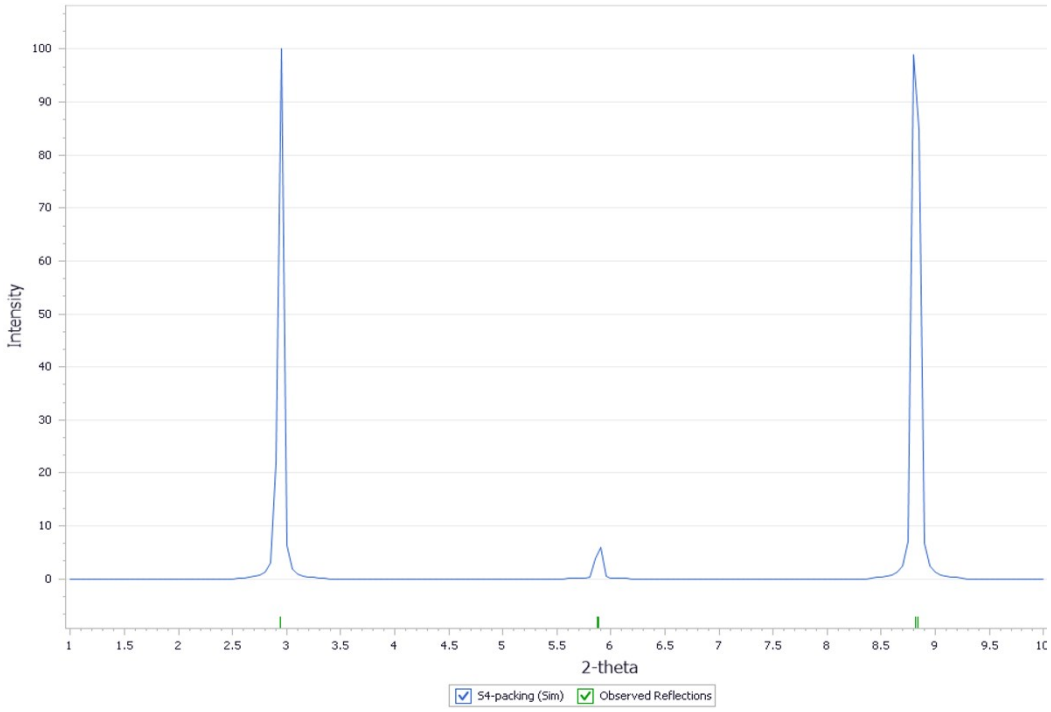

(a)

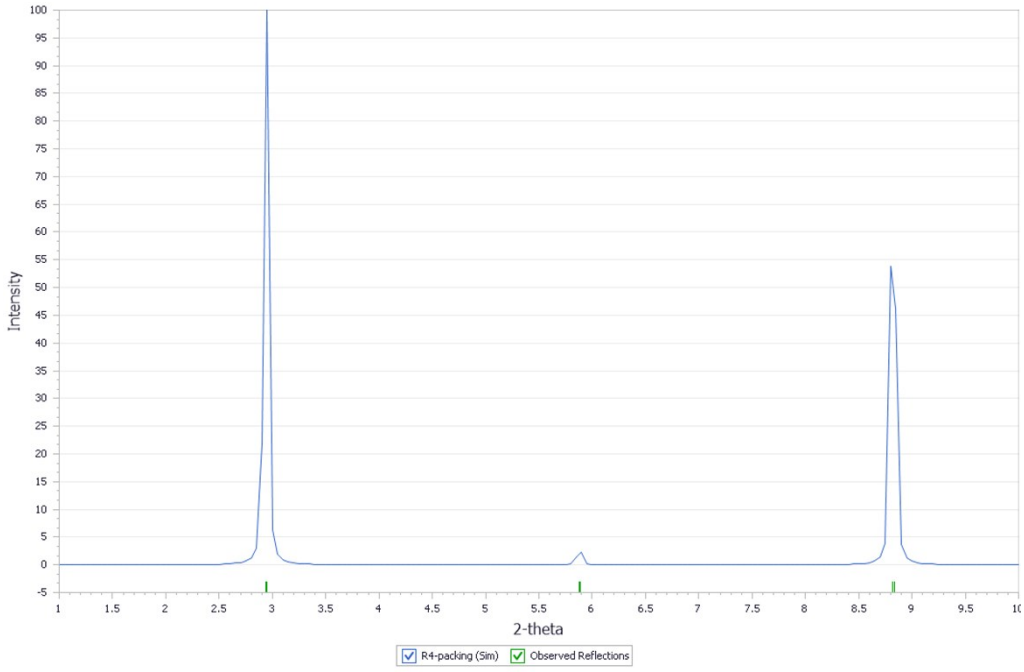

(b)

Figure S16. Simulated XRD patterns for (a) **S4** and (b) **R4** according to experimental data

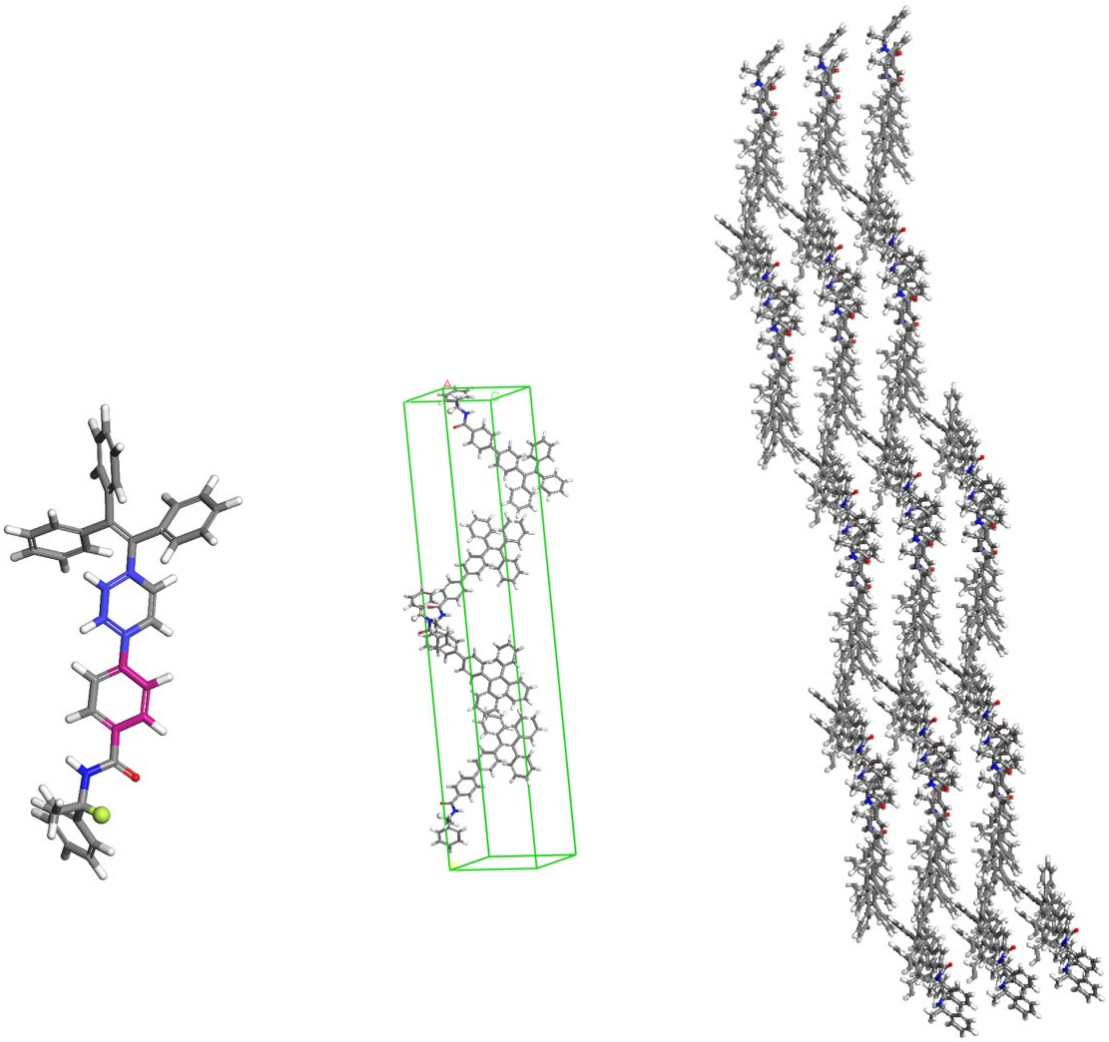

Figure S17. Predicted packing model for **S4** based on simulated XRD patterns: (a) molecular structure, (b) packing model for a single unit cell, and (c) packing model for an assembly.

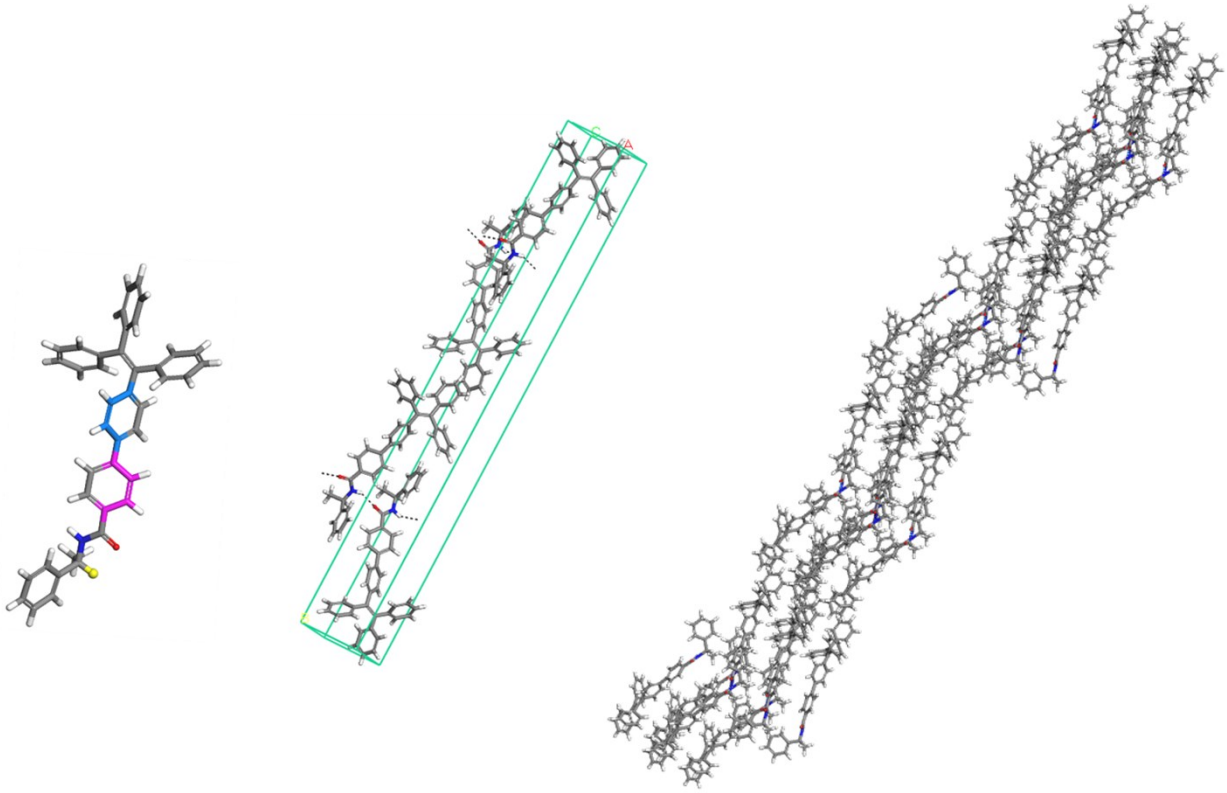

Figure S18. Predicted packing model for **R4** based on simulated XRD patterns: (a) molecular structure, (b) packing model for a single unit cell, and (c) packing model for an assembly.

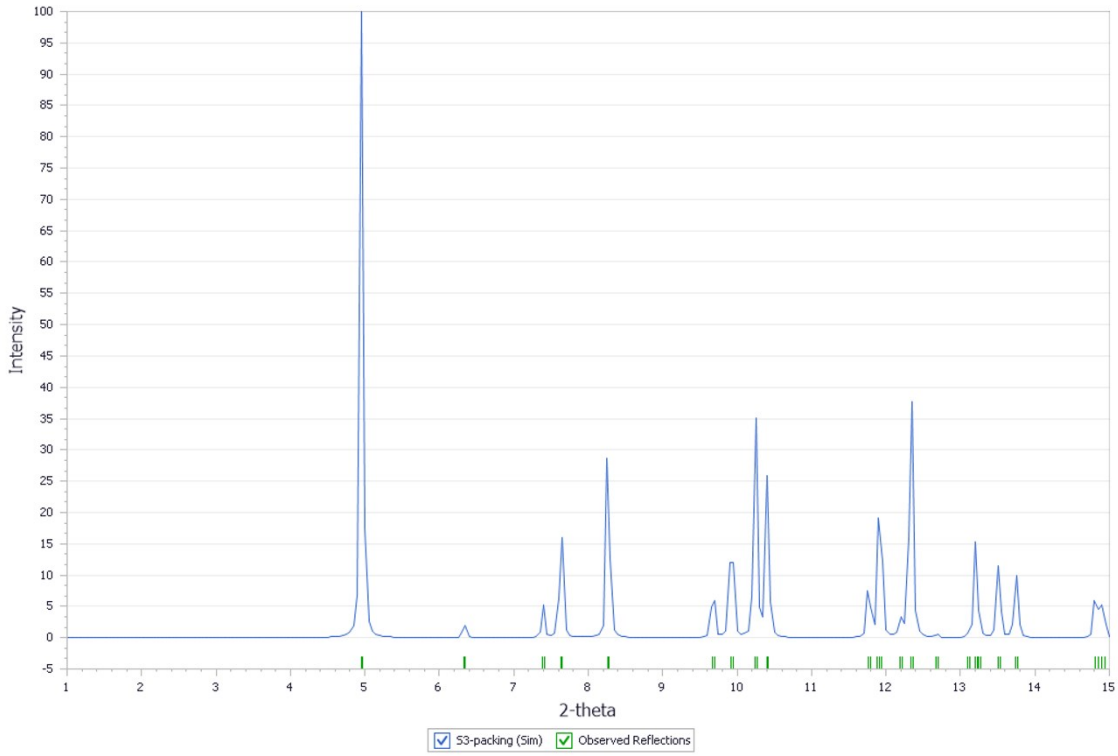

Figure S19. Simulated XRD patterns for **S3** according to experimental data

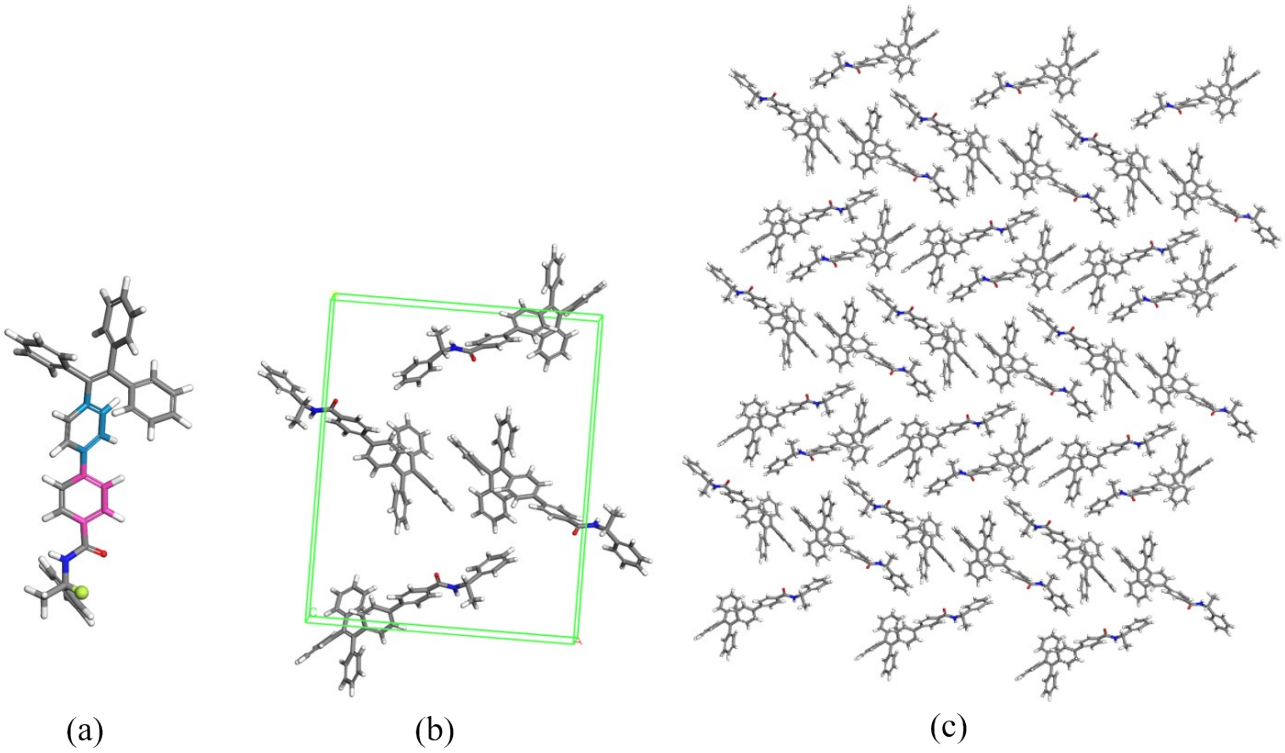

Figure S20. Predicted packing model for **S3** based on simulated XRD patterns: (a) molecular structure, (b) packing model for a single unit cell, and (c) packing model for an assembly.

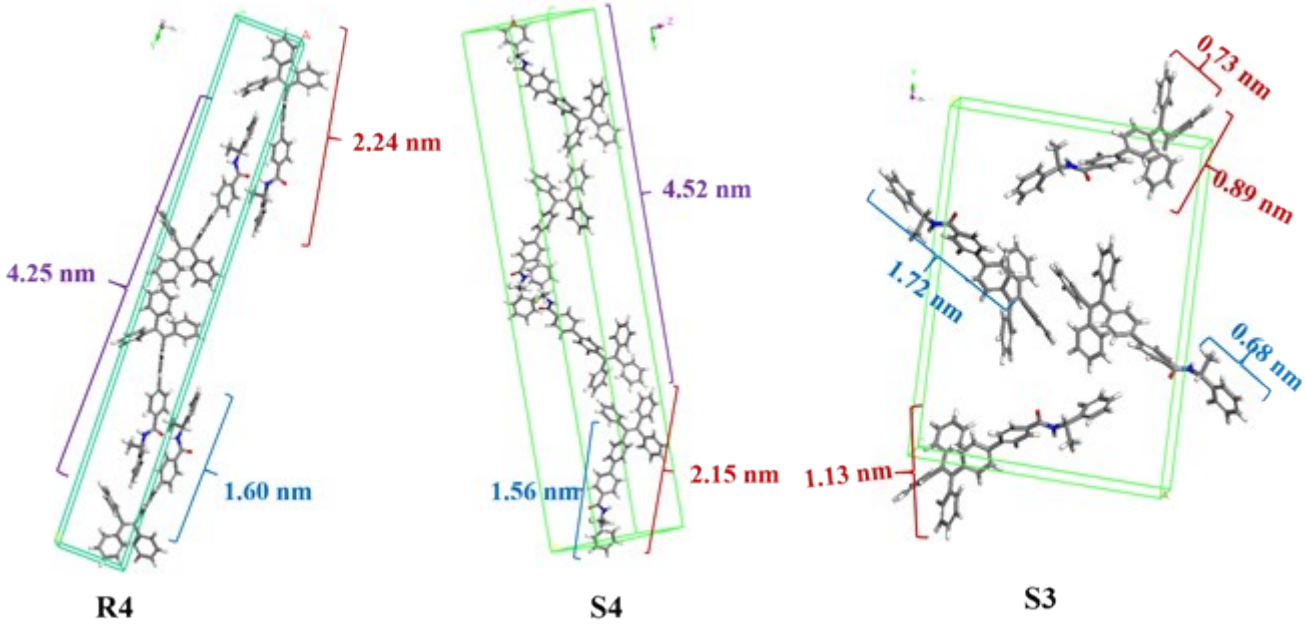

Figure S21. Single unit cells with molecular length for predicted packing models .

3. Other information

3.1 Synthesis

The ***S*-TPE-Ph-PEA** and ***R*-TPE-Ph-PEA** were synthesized according to Scheme S1.

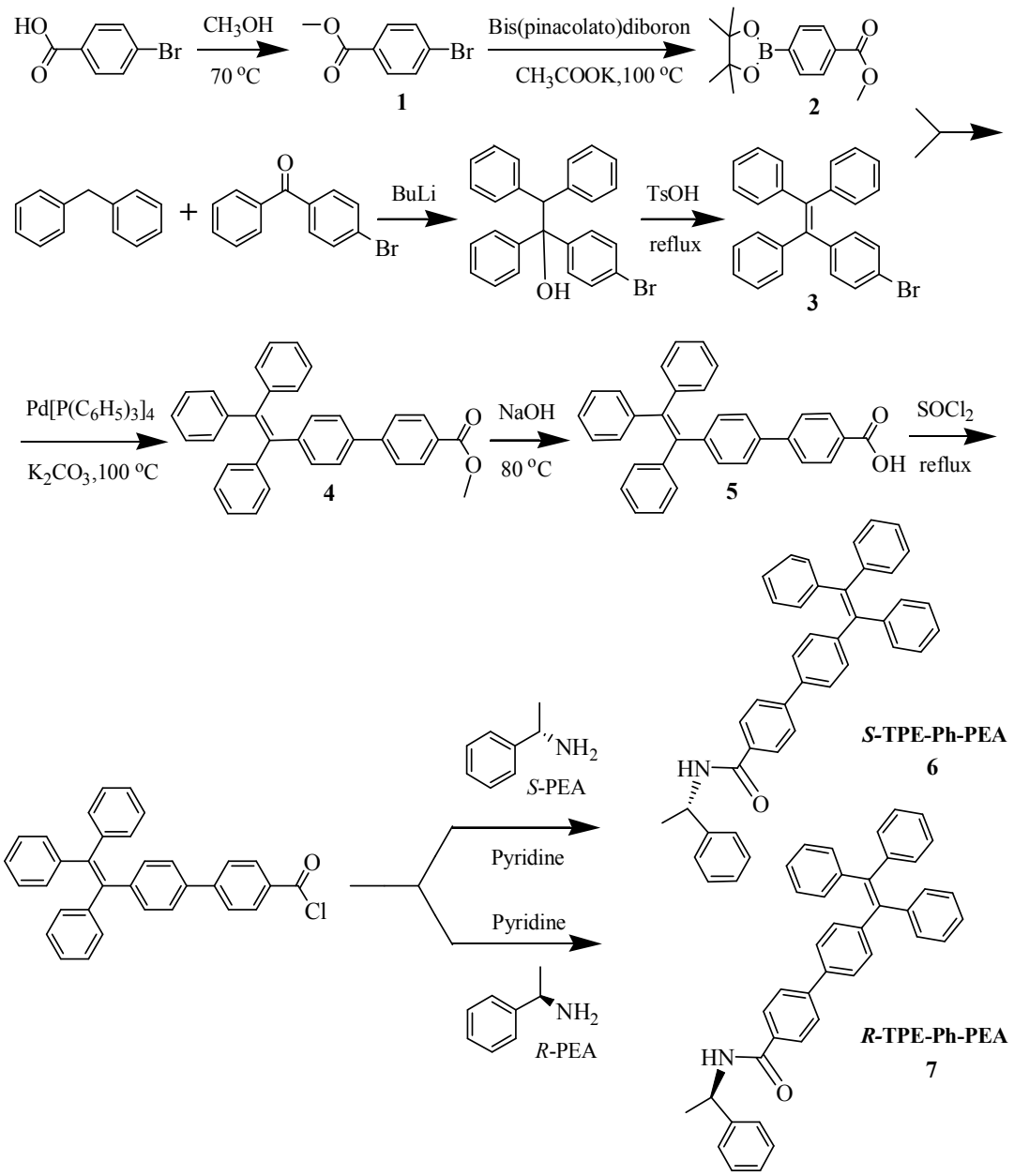

Scheme S1. Synthetic routes for both ***S*-TPE-Ph-PEA** and ***R*-TPE-Ph-PEA** compounds.

Synthesis of methyl 4-bromobenzoate (1). Synthesis methods of compound 1 were according to reference 14. Sulfuric acid (0.5 mL) was added to a suspension of 4-Bromobenzoic acid (4.02 g) in anhydrous methanol (50 mL). The mixture was stirred at 90°C for 24 h and then the residual methanol was removed under reduced pressure. The residue was recrystallized from dichloromethane (CH_2Cl_2) to give a white powder (3.89 g, 91%). ^{1}H NMR (400 MHz, $CDCl_3$) δ 8.01-7.83 (m, 2H; Ar-*H*), 7.67-7.51 (m, 2H; Ar-*H*), 3.92 (s, 3H; OC*H*$_3$).

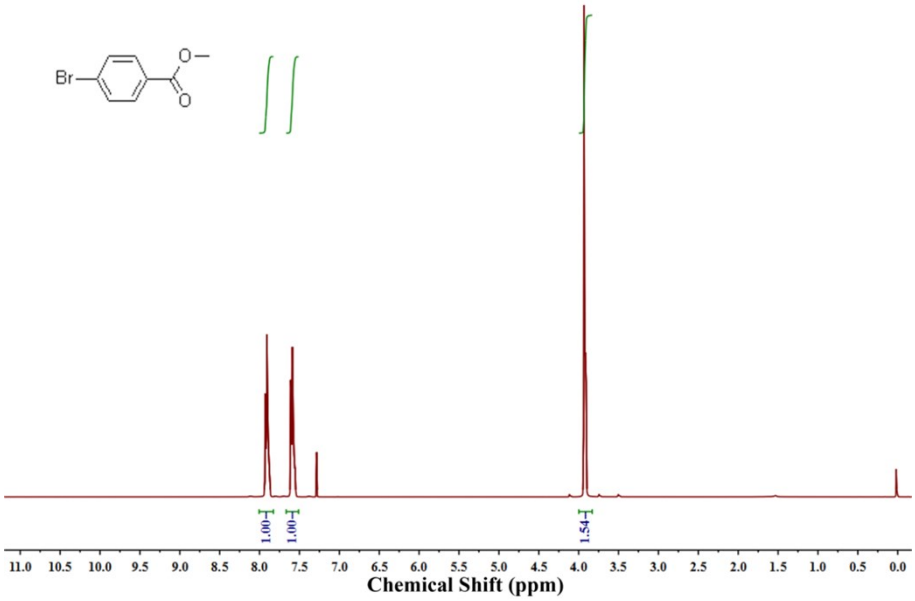

Figure S22. ^{1}H NMR spectrum of compound **1**.

Synthesis of methyl 4-(4,4,5,5-tetramethyl-1,3,2-dioxaborolan-2-yl) benzoate (2). Synthesis methods of compound 2 were according to reference 15. Pd(dppf)Cl_2 (550 mg, 0.71 mmol) was added to a 60 mL dimethyl formamide (DMF) solution of **1** (3.00 g, 14 mmol), bis(pinacolato)diboron (3.9 g, 15.4 mmol) and KOAc (3.9 g, 39 mmol) under argon. The mixture was refluxed overnight. After quenching with aqueous ammonium chloride, the mixture was extracted with CH_2Cl_2. The combined organic layer was washed with brine and dried over anhydrous sodium sulfate. After removal of the solvent at reduced pressure, the residue was purified by column chromatography (silica gel, ethyl acetate/petroleum ether (PE) = 1/8 v/v) to obtain a white solid compound **3** (3.2 g, yield: 88%). ^{1}H NMR (400 MHz, $CDCl_3$) δ 8.08-7.97 (m, 2H; Ar-*H*), 7.92-7.82 (m, 2H; Ar-*H*), 3.93 (s, 3H; OCH_3), 1.36 (s, 12H; OC(CH_3)$_2$).

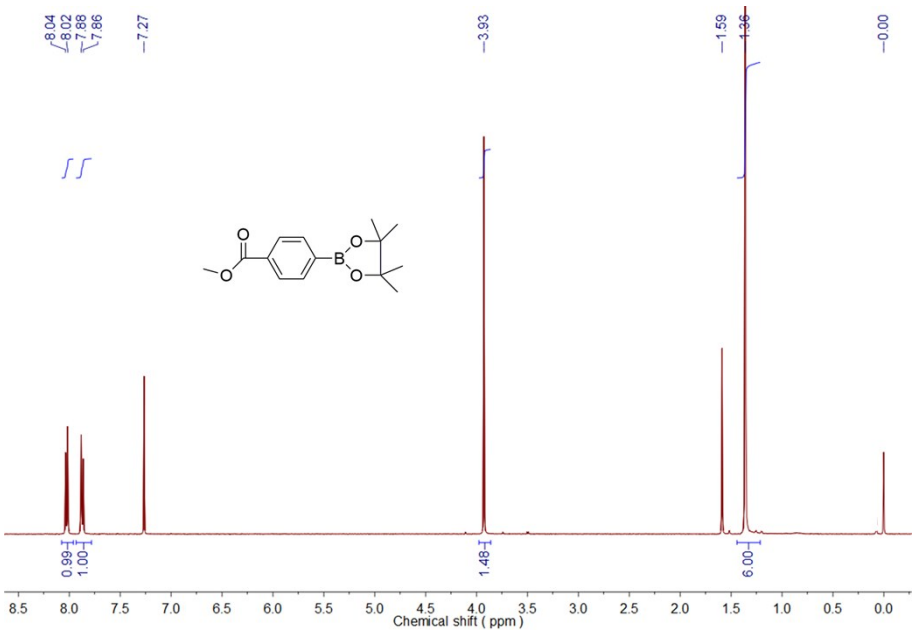

Figure S23. ^{1}H NMR spectrum of compound **2**.

Synthesis of (2-(4-bromophenyl)ethene-1,1,2-triyl)tribenzene (3). A 2.5 M solution of n-butyllithium in hexane (12 mL, 30 mmol) was added to a solution of diphenylmethane (5 g, 30 mmol) in anhydrous tetrahydrofuran (50 mL) at -5°C under argon. After stirring for 2 h, 4-bromobenzophenone (7.76 g, 30 mmol) was added and the reaction mixture was stirred for 12 h to allow the temperature to rise gradually to room temperature. The reaction was quenched with an aqueous solution of ammonium chloride, and the mixture was extracted with CH_2Cl_2. The organic layer was evaporated after drying with anhydrous sodium sulfate and the resulting crude hydroxyl intermediate was dissolved in toluene (100 mL) for subsequent reaction. *p*-Toluenesulfonic acid (0.8 g, 4.7 mmol) was added, and the mixture was refluxed for 12 h and cooled to room temperature. The solvent was evaporated, and the crude product was purified by silica gel column chromatography using DCM/PE (v/v = 1/10) as eluent to yield compound **5** as a white powder (10.8 g, 89%). ^{1}H NMR (400 MHz, $CDCl_3$) δ= 7.22 (d, *J* = 8.4 Hz, 2H, Ar-*H*), 7.12 (m, 9H, Ar-*H*), 7.02-7.04 (m, 6H, Ar-*H*), 6.90 (d, *J* = 8.4 Hz, 2H, Ar-*H*).

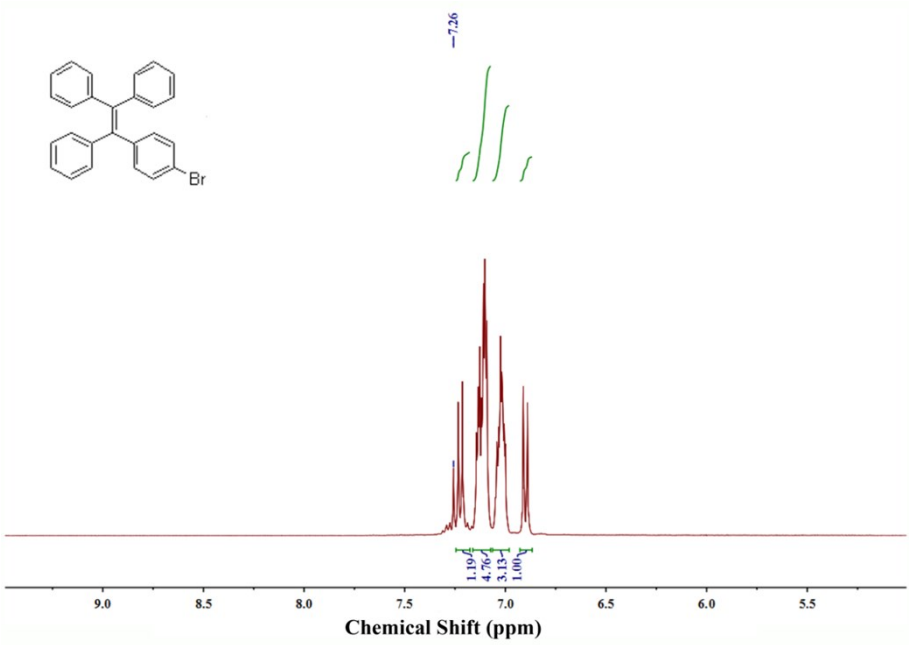

Figure S24. ^{1}H NMR spectrum of compound **3**.

Methyl 4'-(1,2,2-triphenylvinyl)-[1,1'-biphenyl]-4-carboxylate (4). Into a solution of compound **2** (1.31 g, 5 mmol) and compound **3** (2.1 g, 5 mmol) in 12 mL potassium carbonate (2 M, aq.) solution mixed with 30 mL THF and 8 mL ethanol, tetrakis(triphenylphosphine)palladium (0) (173.5 mg, 0.15 mmol) was added under argon atmosphere. The reaction temperature was increased to 100°C and the mixture was stirred for 24 h. The solution was concentrated by a rotary evaporator and extracted with CH_2Cl_2. The organic layer was separated and washed with brine, dried over anhydrous magnesium sulfate, and the solvent was evaporated to dryness under reduced pressure. The crude product was purified using a silica gel column with DCM/PE (v/v = 1/6) as eluent. Product **4** was obtained with 83% yield (1.93 g). ^{1}H NMR (400 MHz, $CDCl_3$) δ 8.05 (t, *J* = 6.9 Hz, 2H; Ar-*H*), 7.61 (d, *J* = 8.4 Hz, 2H; Ar-*H*), 7.38 (d, *J* = 8.3 Hz, 2H; Ar-*H*), 7.16-7.01 (m, 17H; Ar-*H*), 3.93 (s, 3H; C*H*$_3$).

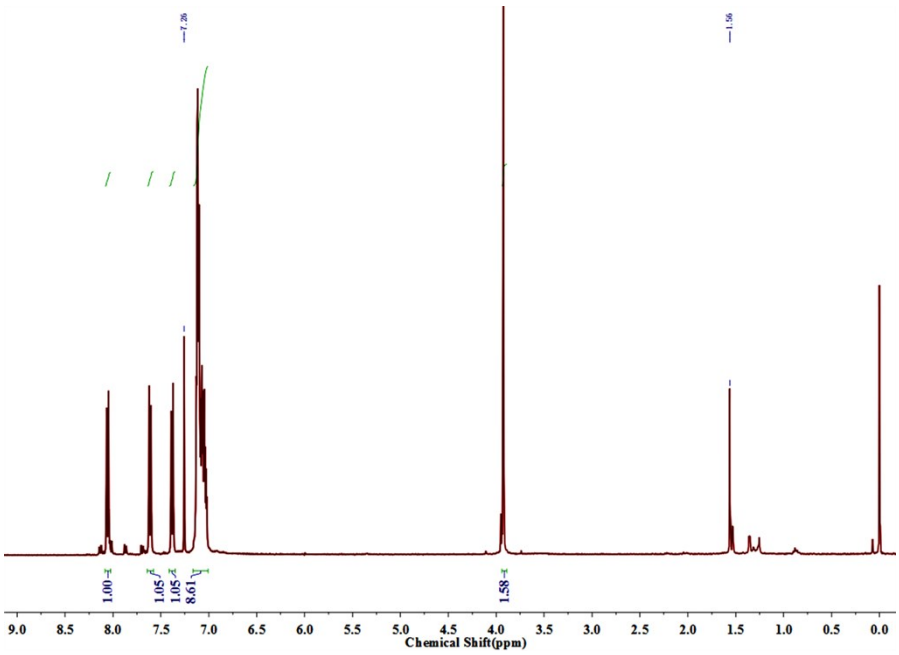

Figure S25. ^{1}H NMR spectrum of compound **4**.

Synthesis of 4'-(1,2,2-triphenylvinyl)-[1,1'-biphenyl]-4-carboxylic acid (5). Compound **4** (1.86 g, 4 mmol) was dissolved in 50 mL THF, then 30 mL water and sodium hydroxide (0.2 g) were added. The solution was placed in a nitrogen atmosphere and heated to 80°C with vigorous stirring for 36 h. The solution was concentrated by a rotary evaporator and extracted with CH_2Cl_2. The organic layer was separated and washed with brine, dried over anhydrous magnesium sulfate, and evaporated to dryness under reduced pressure. The crude product was recrystallized from methanol to give 4-(4-formic acid phenyl) tetraphenyl ethylene (compound **5**) as a white powder (1.55 g, 86%). ^{1}H NMR (400 MHz, DMSO-d6) δ 12.93 (d, J = 14.4 Hz, 1H; COO*H*), 7.95 (d, *J* = 6.6 Hz, 2H; Ar-*H*), 7.72 (s, 2H; Ar-*H*), 7.53 (d, *J* = 6.5 Hz, 2H; Ar-*H*), 7.25-6.83 (m, 17H; Ar-*H*).

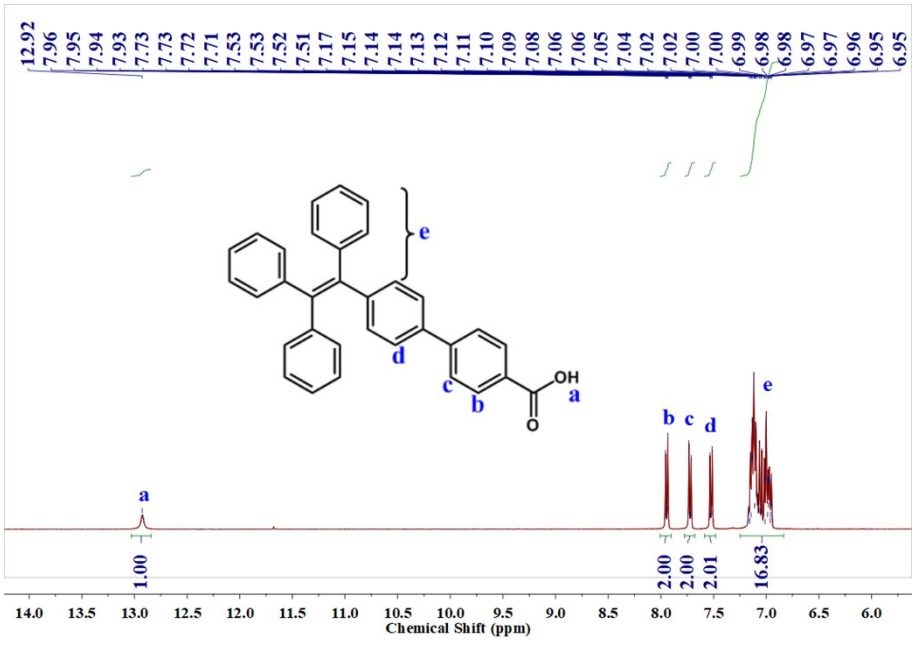

Figure S26. ^{1}H NMR spectrum of compound **5**

Synthesis of *S*-TPE-Ph-PEA and ***R*-TPE-Ph-PEA** (**6 and 7**). Compound **5** (1.35 g, 3 mmol) was dissolved in 20 mL THF, 2 mL thionyl chloride added at room temperature and then heated to 70°C with vigorous stirring for 4 h. After reaction completed, mixtures were cooled to room temperature and evaporated to dryness under reduced pressure to give a powder. Pyridine (0.4 mL, 5 mmol), dimethylaminopyridine (10 mg), (*S*)- or (*R*)-1-phenylethylamine (0.22 g, 1.8 mmol) were dissolved in 10 mL of THF, and the resulting mixture was then cooled in an ice bath under vigorous stirring for 30 min. The obtained acid chloride powder was dissolved in 5 mL THF and then added dropwise by using a constant-pressure dropping funnel. Afterwards, the mixture was warmed up to room temperature and stirred for 24 h. The solution was concentrated in a rotary evaporator and then extracted with CH_2Cl_2. The organic layer was separated and washed with brine, dried over anhydrous magnesium sulfate, evaporated to dryness under reduced pressure, and then purified by column chromatography on silica gel using 1:7(v/v) EA/PE solution to get the target compounds (**6**, 0.63 g, 76%; **7**, 0.58 g, 70%).

***S*-TPE-Ph-PEA** (**6**): ^{1}H NMR (400 MHz, $CDCl_3$) δ 7.83 (d, *J* = 8.5 Hz, 2H; Ar-*H*), 7.61 (d, *J* = 8.4 Hz, 2H; Ar-*H*), 7.46-7.35 (m, 6H; Ar-*H*), 7.34-7.30 (m, 1H; Ar-*H*), 7.13-6.93 (m, 17H; Ar-*H*), 6.33 (d, *J* = 7.7 Hz, 1H; CON*H*), 5.45-5.35 (m, 1H; NC*H*), 1.66 (d, *J* = 6.9 Hz, 3H; C*H*$_3$);^{13}C NMR (100 MHz, $CDCl_3$) δ 166.27, 143.75, 143.66, 143.64, 143.20, 141.46, 140.31, 137.62, 133.02, 131.94, 131.41, 131.35, 128.78, 127.84, 127.77, 127.69, 127.49, 127.43, 126.90, 126.62, 126.58, 126.54, 126.32, 49.27, 21.78; HRMS (ESI, m/z) Calcd for $C_{41}H_{33}NO$: 556.263491 [M]+. Found: 556.26338.

***R*-TPE-Ph-PEA** (**7**) ^{1}H NMR (400 MHz, $CDCl_3$) δ 7.80 (d, *J* = 8.2 Hz, 2H; Ar-*H*), 7.60 (d, *J* = 8.2 Hz, 2H; Ar-*H*), 7.45-7.33 (m, 6H; Ar-*H*), 7.33-7.27 (m, 1H; Ar-*H*), 7.20-6.95 (m, 17H; Ar-*H*), 6.33 (d, *J* = 7.8 Hz, 1H; CON*H*), 5.41-5.33 (m, 1H; NC*H*), 1.63 (d, *J* = 6.8 Hz, 3H; C*H*$_3$); ^{13}C NMR (100 MHz, $CDCl_3$) δ 166.36, 143.69, 143.69, 143.66, 143.28, 141.49, 140.35, 137.65, 133.05, 131.97, 131.44, 131.39, 128.78, 127.88, 127.81, 127.73, 127.51, 127.48, 126.90, 126.66, 126.62, 126.58, 126.35, 49.30, 21.82; HRMS (ESI, m/z) Calcd for $C_{41}H_{33}NO$: 556.263491 [M]+. Found: 556.263491.

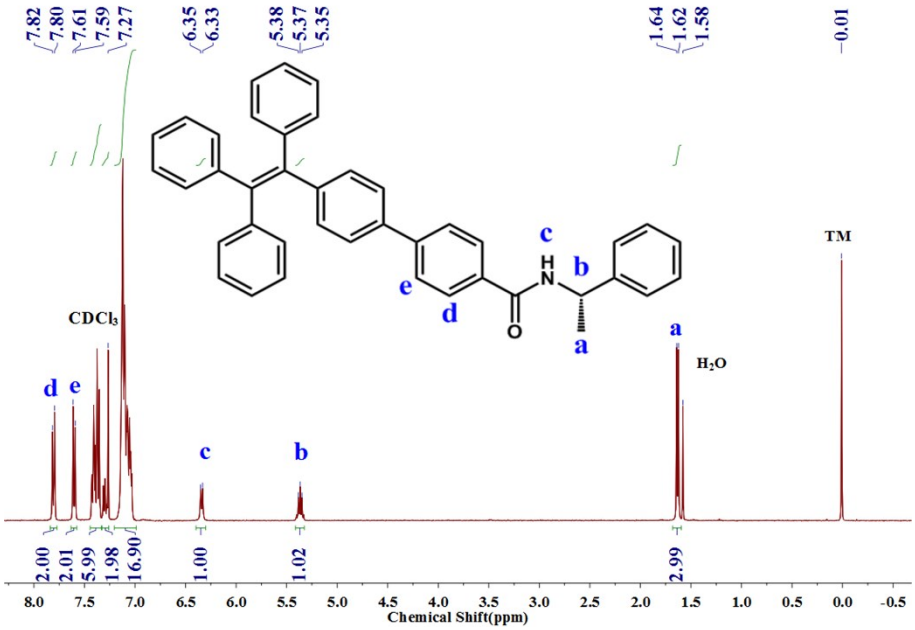

Figure S27. [1]H NMR spectrum of compound **6**, ***S*-TPE-Ph-PEA.**

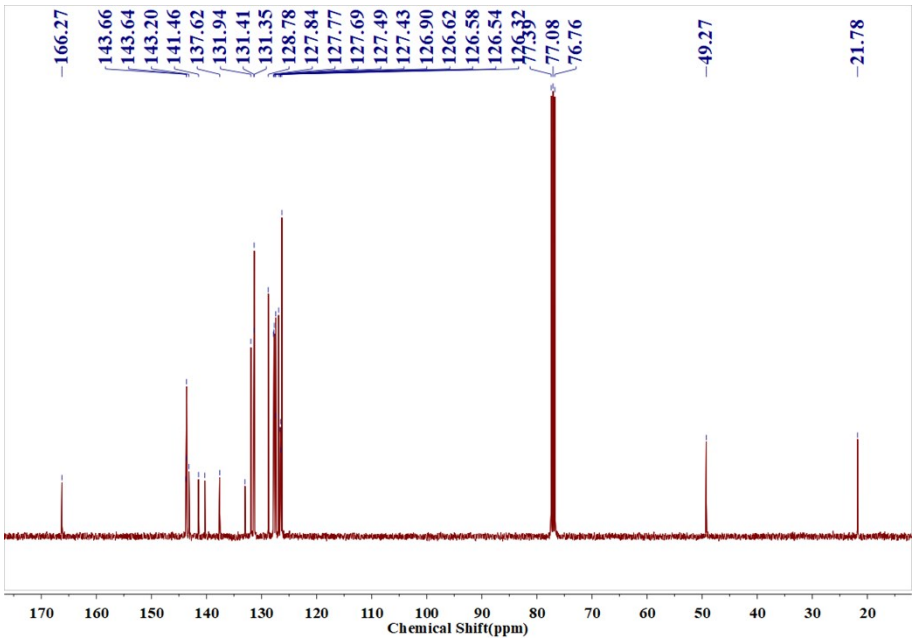

Figure S28. [13]C NMR spectrum of compound **6**, ***S*-TPE-Ph-PEA.**

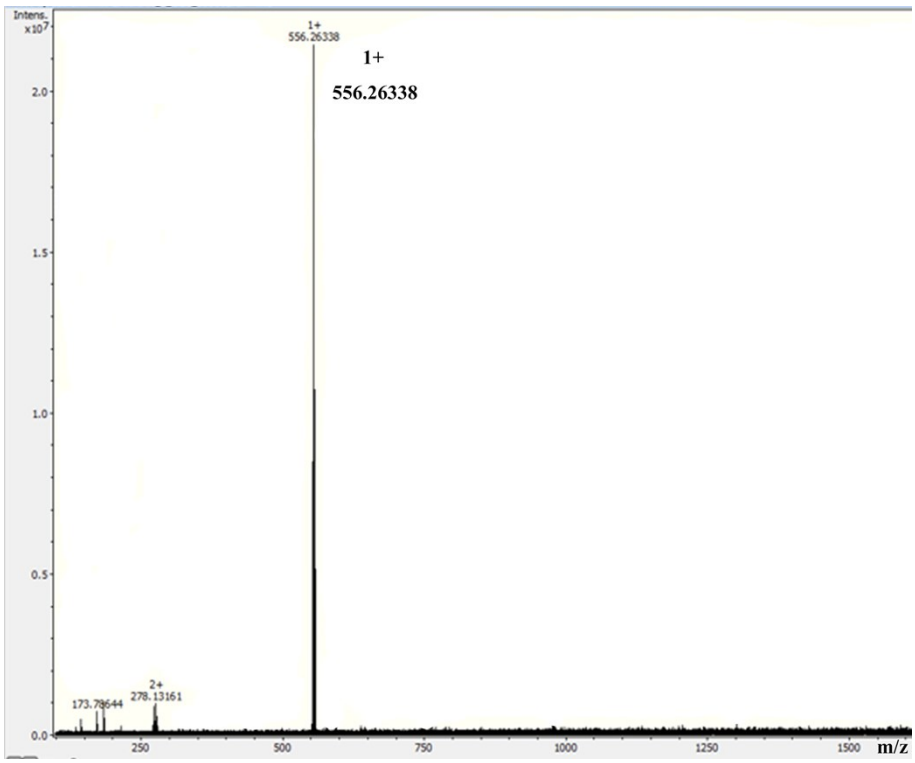

Figure S29. HRMS spectrum of compound **6**, ***S*-TPE-Ph-PEA**.

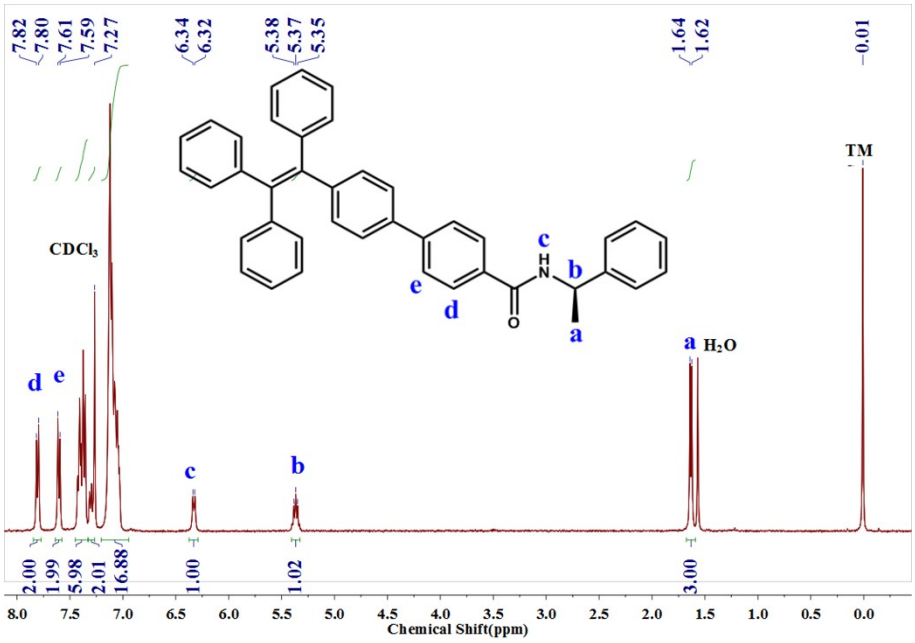

Figure S30. ^{1}H NMR spectrum of compound **7**, ***R*-TPE-Ph-PEA.**

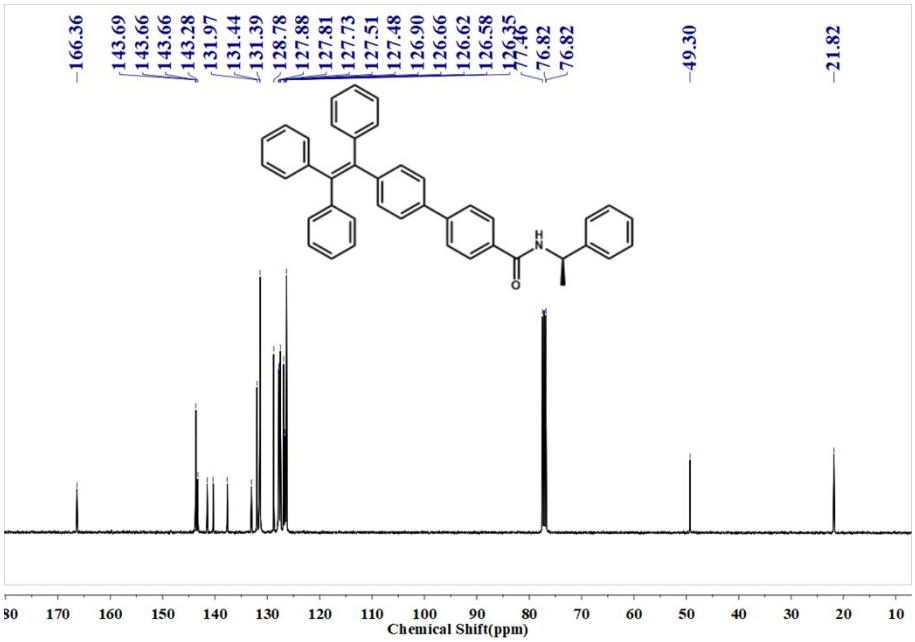

Figure S31. ^{13}C NMR spectrum of compound **7**, ***R*-TPE-Ph-PEA.**

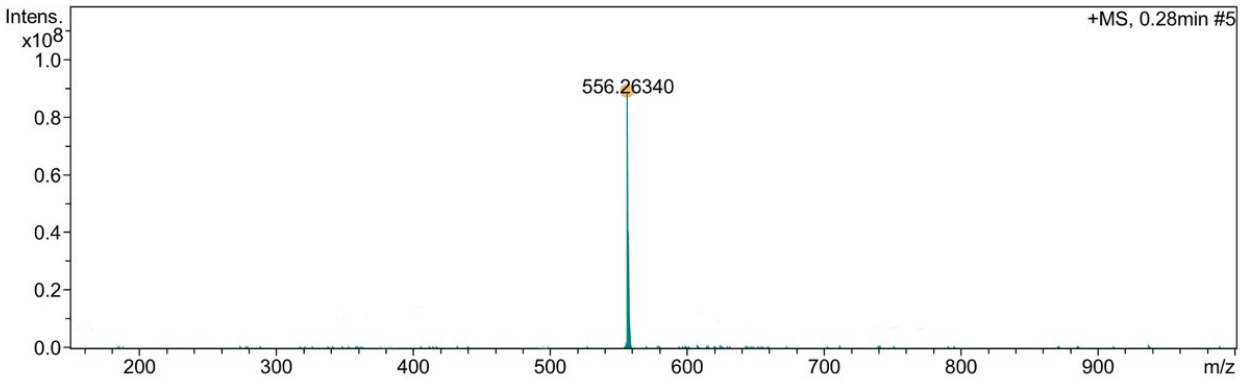

Figure S32. HRMS spectrum of compound **7**, ***R*-TPE-Ph-PEA**.

References

[1] N. Metropolis, A. W. Rosenbluth, M. N. Rosenbluth, A. H. Teller, E. Teller, *J. Chem. Phys.* **1953**, *21*, 1087.

[2] S. W. Bunte, H. Sun, *J. Phys. Chem. B* **2000**, *104*, 2477.

[3] a) A. Klamt, G. Schueuermann, *J. Chem. Soc., Perkin Trans. 2* **1993**, 799; b) J. Tomasi, M. Persico, *Chem. Rev.* **1994**, *94*, 2027.

[4] J. P. Perdew, Y. Wang, *Phys. Rev. B* **1992**, *45*, 13244.

[5] J. Andzelm, R. D. King-Smith, G. Fitzgerald, *Chem. Phys. Lett.* **2001**, *335*, 321.

[6] N. Govind, M. Petersen, G. Fitzgerald, D. King-Smith, J. Andzelm, *Comput. Mater. Sci.* **2003**, *28*, 250.

[7] D. K. Dhaked, V. Jain, Y. Kasetti, P. V. Bharatam, *Struct. Chem.* **2012**, *23*, 1857.

[8] a) A. Arslantas, *Int. J. Mol. Sci.* **2005**, *6*, 291; b) F. Leusen, *J. Cryst. Growth* **1996**, *166*, 900; c) S. Price, *Phys. Chem. Chem. Phys.* **2008**, *10*, 1996; d) S. M. Reed, T. J. R. Weakley, J. E. Hutchison *Crystal Engineering* **2000**, *3*, 85; e) J. R. Smith, W. Xu, D. Raftery, *J. Phys. Chem. B* **2006**, *110*, 7766; f) T. V. Timofeeva, T. Kinnibrugh, O. Y. Borbulevych, B. B. Averkiev, V. N.

Nesterov, A. Sloan, M. Y. Antipin, *Cryst. Growth Des.* **2004**, *4*, 1265.
[9] R. L. C. Akkermans, N. A. Spenley, S. H. Robertson, *Mol. Simul.* **2013**, *39*, 1153.
[10] V. K. Bel'skii, P. M. Zorkii, *Acta Crystallogr., Sect. A* **1977**, *A33*, 1004.
[11] a) W. H. Baur, D. Kassner, *Acta Cryst. B*, 1992, **48**, 356-369; b) A. Boultif, D. Louër, *J. Appl. Cryst.*, 1991, **24**, 987.
[12] IUPAC-IUB Commission on Biochemical Nomenclature, *Biochemistry* **1970**, *9*, 3471.
[13] a) B. Delley, *J. Chem. Phys.* **1990**, *92*, 508; b) B. Delley, *J. Phys. Chem.* **1996**, *100*, 6107.
[14] a) L. Wang, J. Li, X. Cui, Y. Wu, Z. Zhu, Y. Wu, *Adv. Synth. Cat.*, 2**010**, 352, 2002; b) Q. Ye, S. Chen, D. Zhu, X. Lu, Q. Lu, *J. Mater. Chem. B* **2015**,3, 3091.
[15] Q. Zhao, S. Zhang, Y. Liu, J. Mei, S. Chen, P. Lu, A. Qin, Y. Ma, J. Z. Sun, B. Z. Tang, *J. Mater. Chem.* **2012**, 22, 7387.